Sensors and Materials, Vol. 34, No. 9 (2022) 3397–3409
MYU Tokyo

S & M 3048

Vector Magnetic Gradiometer with Adjustable Gradient Sensitivity Based on Anisotropic Magnetoresistance

Chao Tan,* Xianzhi Ye, Qihao Sun, Liang Xin,
Long Yang, Junming Duan, and Haoran Chen

College of Electrical Engineering & New Energy, China Three Gorges University, Yichang 443002, China

(Received June 10, 2022; accepted August 16, 2022)

Keywords: AMR gradiometer, magnetic field gradient, signal-to-noise, sensitivity

In this study, an anisotropic magnetoresistance (AMR) vector magnetic gradiometer with adjustable gradient sensitivity was developed to measure the magnitude of the vector magnetic field gradient. First, two AMR chip sensors were used to construct the measurement probe of the magnetic gradiometer, and a signal-conditioning circuit based on proportional integral closed-loop control was designed to create a vector magnetic gradiometer with adjustable gradient sensitivity. Next, by using the circuit diagram of the AMR vector magnetic gradiometer, the measurement principle of the AMR vector magnetic gradiometer was theoretically studied, the relationship between the magnetic field gradient and the output voltage of the AMR vector magnetic gradiometer was obtained, and the noise of the AMR vector magnetic gradiometer was analyzed. Finally, a gradient test platform was constructed to test the magnetic field gradient measurement performance of the AMR vector magnetic gradiometer. The experimental results revealed that when the feedback resistance of the *V*/*I* conversion circuit of the AMR vector magnetic gradiometer is 200 Ω, the noise level is 122.36 pT/Hz$^{1/2}$ at 1 Hz, and the nonlinearity and gradient sensitivity are 0.9968% and 11.707 μV/(nT/m), respectively. The proposed gradiometer can be used to measure the gradient of the input magnetic field, and its interesting application is the gradiometer to measure magnetic field anomalies in the presence of large uniform magnetic field disturbances.

1. Introduction

As an effective means of magnetic anomaly detection, magnetic field gradient measurement has been widely employed in earth resource exploration, biomagnetic field measurement, nondestructive testing, unexploded ordnance detection, and magnetic potential detection and detonators.[1–7] With higher standards for the detection sensitivity of magnetic anomalies in science and engineering applications, the requirements for the sensitivity and noise of magnetometers have been further increased.

Magnetic field gradient measurement involves two quantities: (1) the total-field gradient, which is generally obtained by subtracting the measurement results of two total-field

*Corresponding author: e-mail: ctgutc@ctgu.edu.cn
https://doi.org/10.18494/SAM3989

ISSN 0914-4935

gradiometers separated by a certain distance, and (2) the vector-field gradient, which is usually measured using a vector-field gradiometer. The spatial rate of change of the three magnetic field components T_x, T_y, and T_z of a magnetic field vector T is measured, with a total of nine elements for the measurement of the magnetic field gradient tensor. Generally, a vector gradient magnetometer is used to measure the magnetic field gradient tensor components.[8–10] Ichihara *et al*. designed a total-field gradiometer for measuring magnetic card signals by using two sets of optical pump probes and drivers combined with a signal processing unit. This differential type of measurement eliminates the environmental magnetic noise and improves the signal-to-noise ratio of the gradiometer system.[11] To detect magnetic foreign bodies in lithium-ion batteries, Tanaka *et al*. designed a dual-channel gradiometer system by using two SQUID gradiometers combined with a cryostat to detect small iron particles (*diameter* < 100 μm). Although a SQUID gradiometer has high measurement accuracy, its low-temperature use environment makes the measurement process complex and expensive.[12]

Elrefai *et al*. designed a plate-level fluxgate vector gradiometer with a gradient sensitivity of 3.77 μV/(nT/m) and a resolution of 0.39 nT/m; however, the sensor must be designed separately, the gradiometer is difficult to mass produce, and measurement results are inconsistent.[13] To measure weak magnetic fields under unshielded conditions, Riveros *et al*. designed a vector gradiometer by using giant magneto-impedance (GMI); when the probe baseline distance was 6 cm, the sensitivity was 5.94 μV/(nT/m) and a resolution of 833.33 nT/m within a 500 Hz bandwidth was obtained.[14] To measure the geomagnetic field gradient tensor, Sui *et al*. designed a magnetic field gradient tensor measurement system by using multiple fluxgate gradiometers along with a calibration method; this improved the accuracy of each gradient tensor component.[15] Furthermore, to measure the magnetic field gradient tensor component, Merayo *et al*. designed a vector gradiometer by using a dual-channel fluxgate and a spherical feedback coil, achieving a gradient resolution of 0.1 nT/m.[16] However, the dual-channel structure of the gradiometer yields inconsistent measurement results.

In this study, an integrated AMR chip was used to design a low-cost gradient magnetometer with adjustable sensitivity because it offers the following advantages:

1) The design complexity is low, thereby facilitating mass production.
2) The output sensitivity is adjustable.

2. Structure and Operation of Anisotropic Magnetoresistance (AMR) Vector Magnetic Gradiometer

2.1 Sensor structure

The proposed AMR vector magnetic gradiometer consists of a gradient measurement probe and a signal-conditioning circuit (Fig. 1). The size of the HMC1001 AMR chip sensor is 9.829 × 5.014 × 1.371 mm^3, and the chip comprises a Wheatstone bridge, an offset strap, and a set/reset coil. The AMR chip sensors G_1 and G_2 are soldered on a 12-cm-long probe circuit board, and the distance between G_1 and G_2 is the baseline distance d (10 cm).

A schematic of the AMR vector magnetic gradiometer measurement is shown in Fig. 2. A gradient magnetic field is generated around the energized straight wire, and the AMR vector

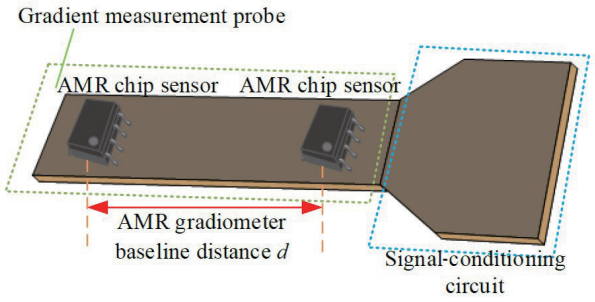

Fig. 1. (Color online) Structure of the AMR vector magnetic gradiometer.

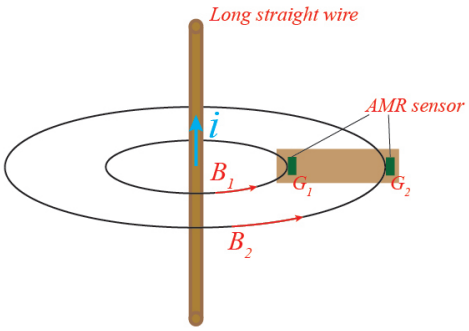

Fig. 2. (Color online) Gradient measurement performed using the AMR vector magnetic gradiometer.

magnetic gradiometer is placed in the gradient magnetic field. The magnetic field gradient at the midpoint of the G_1 and G_2 axes can be expressed as

$$T = \frac{\partial B}{\partial x} = \frac{B_1 - B_2}{d}, \tag{1}$$

where B_1 and B_2 are the magnetic field strength of the energized straight wire at G_1 and G_2, respectively.

2.2 Signal-conditioning circuit and its working mechanism

The signal-conditioning circuit of the AMR vector magnetic gradiometer consists of a preamplifier module, a differential amplifier module, a synchronous detection module, an asynchronous clock, an interal module, a *V*/*I* conversion circuit, and a low-pass filter (Fig. 3).

The dynamic waveform produced when the circuit is operational is shown in Fig. 4. The working mechanism is as follows. Two preamplifiers amplify the weak voltage signal outputted by the AMR chip sensor on the gradient measurement probe. The differential amplifier then differentially amplifies the output of the two preamplifiers and outputs the integrated voltage after phase-sensitive detection (PSD) and integration. The *V*/*I* conversion circuit converts the integrated voltage into a feedback current and acts on the offset strap of the AMR chip sensor.

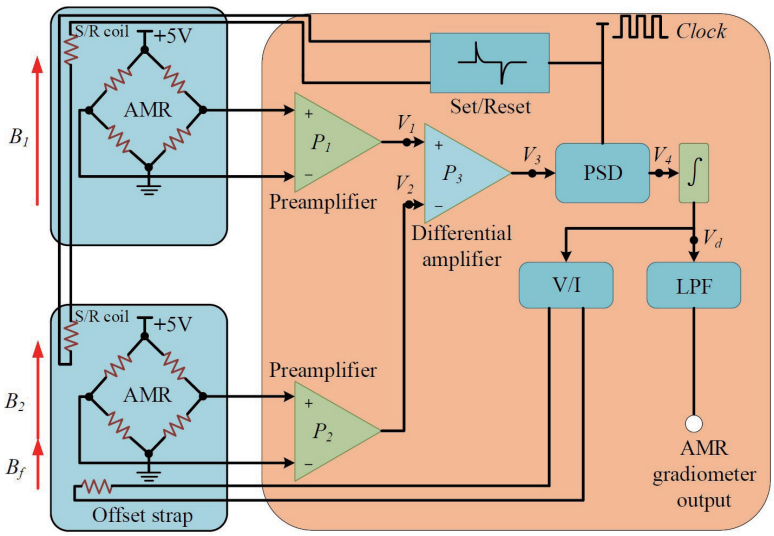

Fig. 3. (Color online) Circuit diagram of the AMR vector magnetic gradiometer.

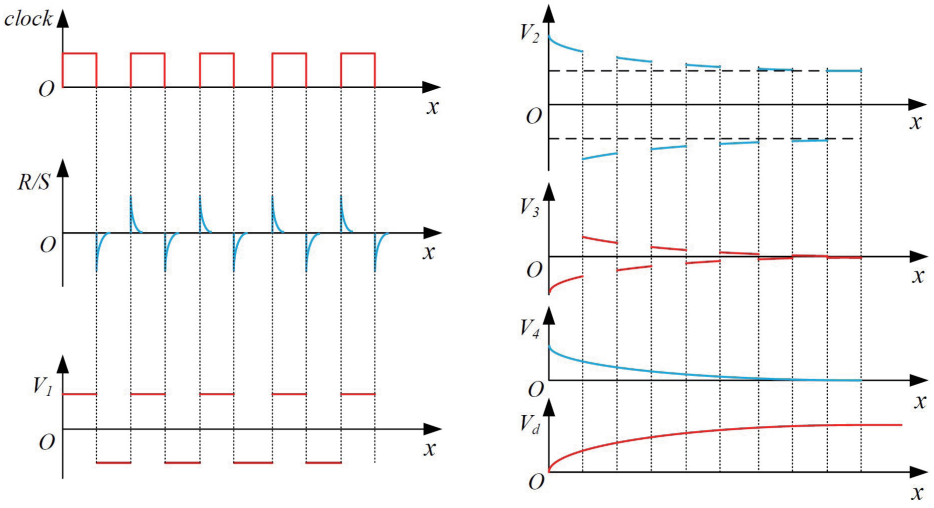

Fig. 4. (Color online) Dynamic waveform of the AMR vector magnetic gradiometer.

The offset strap generates a feedback magnetic field B_f in the same direction as the measured magnetic field B_2. The resultant magnetic field expands and is affected by the output of the feedback sensor. The output voltage of the differential amplifier gradually decreases, whereas that of the integrating circuit continues to increase. When the integral voltage is increased to the maximum value, the combined magnetic field of the feedback magnetic field B_f generated by the offset strap and the measurement magnetic field B_2 is the same as the measurement magnetic field B_1; at this time, the output of the differential amplifier is 0 and the output voltage of the interal circuit no longer increases. Furthermore, the magnitude of the integral voltage is proportional to the feedback magnetic field ΔB.

2.3 Measurement principle

The typical sensitivity of HMC1001 given in the datesheeet is 3.2 mV/V/Gauss, its sensitivity is controlled by the bridge voltage V_{bias}, and when V_{bias} = 5 V, S_{AMR} = 16 mV/Gauss. As can be seen from the circuit diagram of the AMR vector magnetic gradiometer (or AMR gradiometer) in Fig. 2, the integral voltage V_d is converted into the feedback current I by the V/I conversion circuit and the feedback current outputted by the V/I conversion circuit can be expressed as

$$I = V_d/R, \tag{2}$$

where R is the feedback resistance.

The relationship between the feedback magnetic field B_I and the feedback current I can be expressed as

$$B_I = I/k, \tag{3}$$

where k = 51 mV/Gauss is the coil constant of the offset strap.

Owing to the variation in the fabrication accuracy of the sensors, the sensitivity coefficient of each sensor is different; to compensate for sensitivity bias, the gradiometer is placed in a uniform magnetic field, and the gain of the preamplifiers P_1 and P_2 is adjusted to make the differential amplifier P_3 output voltage V_3 equal to zero. The adjusted gradiometer can be used to determine the integrated voltage V_d:

$$V_d = kR(B_1 - B_2). \tag{4}$$

By combining Eqs. (1) to (4), we can determine the relationship between the magnetic field gradient T and V_d as

$$T = V_d/kRd. \tag{5}$$

According to Eq. (5), the gradient outputted by the gradiometer can be changed by adjusting the feedback resistance R and the baseline distance d.

3. Noise Analysis

The gradient sensitivity can be improved by adjusting the gain multiple of the preamplifier or the feedback resistance R. However, adjusting the gain and changing the feedback resistance affect the circuit noise. Therefore, the noise of the AMR gradiometer circuit is analyzed. The effects of changes in preamplifier gain and feedback resistance on the total noise of the circuit are discussed here.

The noise of the AMR gradiometer circuit is caused by thermal, white, shot, and flicker noises of the resistor. The noise sources primarily include the AMR chip sensor, preamplifier,

differential amplifier, detection circuit, integrator circuit, and feedback circuit noises. To analyze the effects of various noises in the AMR gradiometer on the circuit, a typical amplifier noise model is used, which is combined with the AMR gradiometer circuit diagram depicted in Fig. 3, to establish the noise model of the AMR sensor and amplifier, as shown in Fig. 5. The HMC1001 sensor comprises four bridge resistors. The noise added to the circuit is mainly the thermal noise generated by the bridge resistor. Therefore, the sensor is equivalent to an ideal noise-free resistor R_s and a voltage source e_s as the noise model, e_t is the equivalent noise voltage source of the thermal resistance noise, and e_n and i_n are respectively the equivalent noise voltage and equivalent noise current sources of the amplifier.

The root mean square value for a noise voltage source can be expressed as

$$\overline{e} = \sqrt{4KTR\Delta f}\ , \tag{6}$$

where K is the Boltzmann constant (1.38×10^{-23} J/K), T is the thermodynamic temperature (K), R is the resistance (Ω), and Δf is the noise bandwidth (Hz). [17]

The total noise of the first preamplifier circuit can be obtained as

$$e_{n\_in1} = \sqrt{e_{t1}^2 + \left(e_{no1} / k_1\right)^2 + i_{n1}^2 R_S^2 + 4KTR_{g1}}\ , \tag{7}$$

where e_{t1} is the amplifier input voltage noise, e_{no1} is the amplifier output voltage noise, the amplifier gain multiple k_1 is 10, i_{n1} is the amplifier current noise, and the amplifier gain resistance R_{g1} is 5.1 kΩ. According to the data in the AD620 datasheet of the amplifier, e_{n_in1} = 14.42 nV/Hz$^{1/2}$. [18]

The total noise of the second preamplifier circuit can be obtained as

$$e_{n\_in2} = \sqrt{e_{t2}^2 + \left(e_{no} / k_2\right)^2 + i_n^2 R_S^2 + 4KTR_{g2} + e_{V/I}^2}\ , \tag{8}$$

where e_{t2} is the amplifier input voltage noise, e_{no2} is the amplifier output voltage noise, the amplifier gain multiple k_2 is 10, i_{n2} is the amplifier current noise, and the amplifier gain resistance R_{g2} is 5.1 kΩ. The noise $e_{V/I}$ of the *V*/*I* conversion circuit is determined by the thermal noise of resistor R. When R = 200 Ω, the calculated thermal noise is approximately 1.79 nV/Hz$^{1/2}$ and e_{n_in2} is 14.48 nV/Hz$^{1/2}$.

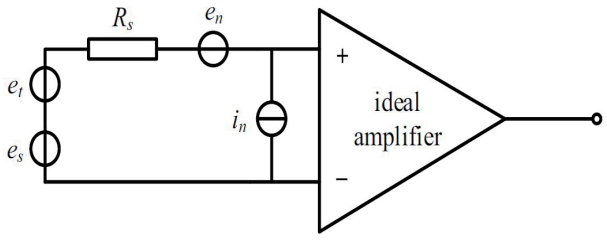

Fig. 5. Noise model of the AMR sensor and preamplifier.

The total noise at the output of the differential circuit can be obtained as

$$E_{n\_out3}=k_3\sqrt{e_{i3}^2+\left(e_{no3}/k_3\right)^2+4KTR_{g3}+k_1^2e_{n\_in1}^2+k_2^2e_{n\_in2}^2}\ . \tag{9}$$

The total voltage noise outputted by the differential circuit is calculated as 550.66 nV/Hz$^{1/2}$. The calculation results revealed that the inherent noise of the AMR chip sensor and the noise of the amplifier account for the highest proportion of the total noise. The effect of the natural noise of the circuit is small, and the change in the real noise of the circuit is notable when the amplifier magnification is changed. Therefore, changing the size of the feedback resistor (R) can minimize changes in circuit noise, thereby improving the gradient sensitivity of the AMR gradiometer. In addition, the appropriate selection of the preamplifier gain and differential amplifier gain plays a key role in determining the total noise of the circuit.

4. Experiment and Analysis

4.1 Experimental test platform

To study the performance of the AMR gradiometer, we developed an experimental test platform to perform noise and gradient sensitivity tests. The magnetic field measurement system of the AMR gradiometer is illustrated in Fig. 6. The functioning generator generates a DC signal to act on a Helmholtz coil. The Helmholtz coil generates a gradient magnetic field after being energized. The Helmholtz coil and the AMR gradiometer were placed in a magnetic shielding cylinder (on a nonmagnetic base) to prevent interference from the external magnetic field. A shielded cable was used to connect the current source with the Helmholtz coil, data acquisition card, and AMR gradiometer. The nonmagnetic base and the shielded cable reduce the interference caused by the noise field and help ensure that the AMR gradiometer only measures the magnetic field generated by the Helmholtz coil. The physical map of the AMR gradiometer is shown in Fig. 7.

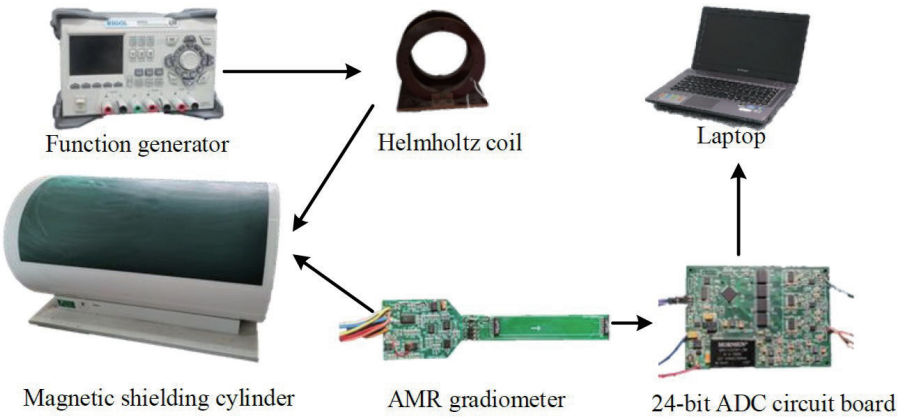

Fig. 6. (Color online) Experimental system for measuring AMR gradiometer magnetic field.

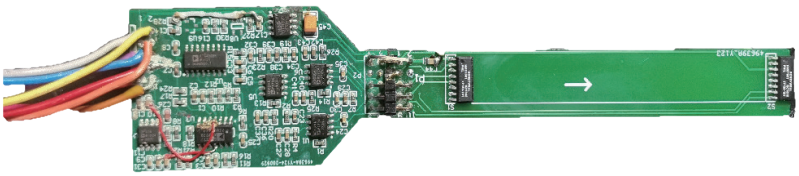

Fig. 7. (Color online) Physical map of the AMR gradiometer.

4.2 Noise test

To analyze the noise performance of the AMR gradiometer, a noise test of the AMR gradiometer was performed in a five-layer magnetic shielding cylinder, and the magnitude of the current passing through the Helmholtz coil was adjusted to generate a magnetic field gradient of approximately 800 nT/cm. Before the measurement, we use a high-sensitivity fluxgate sensor to calculate the gradient magnetic field generated by the Helmholtz coil. The purpose of this is to ensure that the gradient magnetic field measured by the gradiometer is standard. To analyze the measured noise power spectrum of the AMR gradiometer in the magnetic field gradient environment, the system's output data at a sampling rate of 200 Hz was collected, and the magnetic field gradient data outputted by the gradiometer system was recorded at 30 s intervals as the test sample, as shown in Fig. 8.

From Fig. 8, it can be seen that owing to the effects of environmental interference and residual magnetism in the magnetic shielding cylinder, the output magnetic field gradient is slightly greater than 800 nT/cm and the peak-to-peak value of the fluctuation is approximately 0.6 nT/cm. The magnetic field gradient output in the time domain was converted into the frequency domain, and by the spectral analysis of the acquired data, the noise power spectral density was obtained, as shown in Fig. 9. At 5 Hz, the noise of the AMR gradiometer fluctuates at approximately 62 pT/Hz$^{1/2}$. At frequencies above 10 Hz, the noise of the AMR gradiometer fluctuates at approximately 30 pT/Hz$^{1/2}$. The noise of the AMR gradiometer is 122.36 pT/Hz$^{1/2}$ at 1 Hz.

4.3 Gradient sensitivity test

Gradient sensitivity and linearity are important parameters that reflect the performance of the AMR gradiometer. The gradient sensitivity of the AMR gradiometer S_G [unit: μV/(nT/m)] is the ratio of the change in the output voltage signal of the gradiometer to the change in external input magnetic field gradient and can be expressed as

$$S_G = \frac{dV_{out}}{dT}, \tag{10}$$

where V_{out} is the output voltage of the AMR gradiometer and is the magnitude of the magnetic field gradient measured by the AMR gradiometer. We aimed to adjust the magnetic field

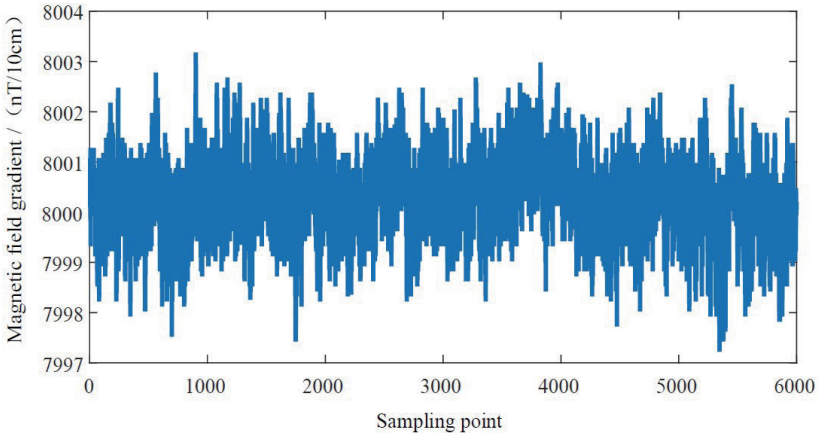

Fig. 8. (Color online) Stable magnetic field gradient output data.

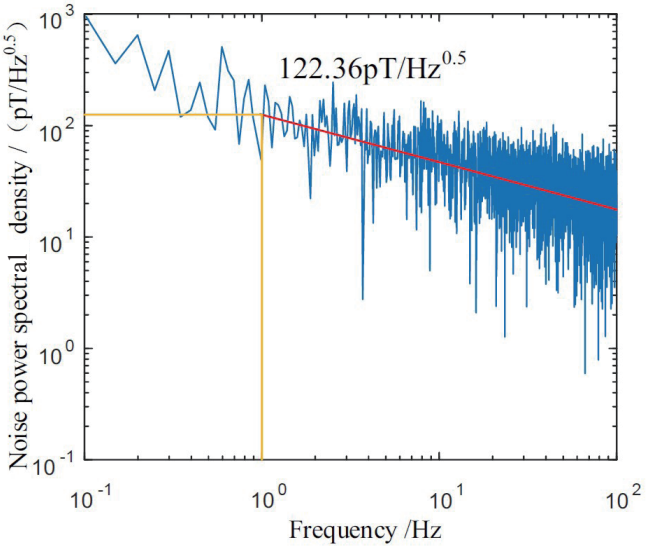

Fig. 9. (Color online) Power spectral density of the AMR gradiometer.

gradient from ±5 × 10^5 nT/m to ±2.5 V. From Eq. (10), the theoretical gradient sensitivity is 5 μV/(nT/m). From Eq. (5), the actual sensitivity of the gradiometer is $S_G = kRd$, and the gradient sensitivity can be changed by adjusting the size of the feedback resistor R in the V/I conversion circuit. To study the linearity of the AMR gradiometer, the magnitude of the current generated by the current source was adjusted, sets of data were collected at a sampling rate of 200 Hz under different currents, and the average of each set of data was used as the output of the current gradiometer. The output scatter plot and fitting result of the instrument are shown in Fig. 10. When R = 91, 150, and 200 Ω under different input gradient magnetic fields, the gradient sensitivities of the gradiometer are 5.7929, 8.5645, and 11.707 μV/(nT/m), respectively.

The fitting residual of the output voltage of the AMR gradiometer when R = 200 Ω is shown in Fig. 11; the maximum residual value is 11.67 mV and the nonlinearity is 0.9968%. The scatter plot of the experimental data and relevant results revealed that the gradient sensitivity of the gradiometer can be improved by adjusting the feedback resistance.

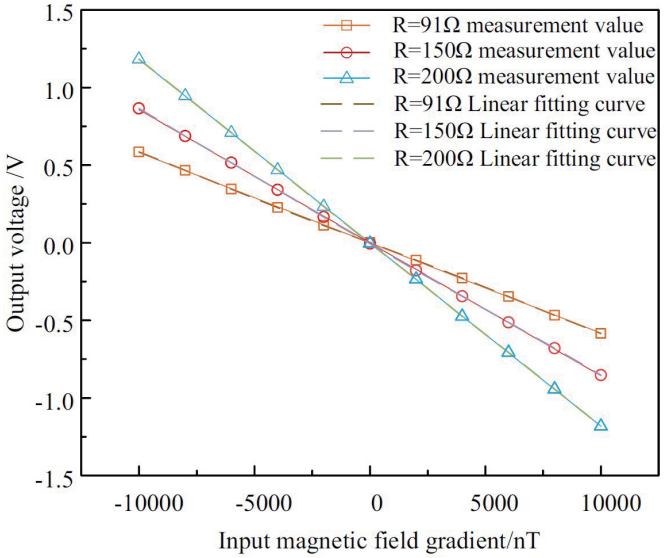

Fig. 10. (Color online) Gradiometer output scatter plot and results of linear fit.

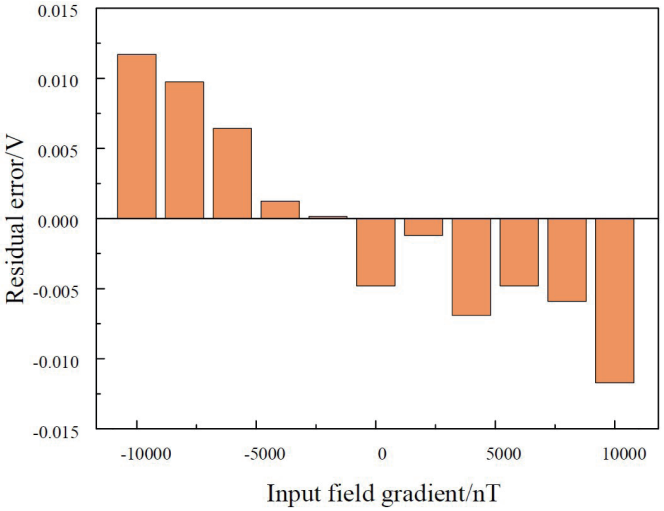

Fig. 11. (Color online) Fitted residuals of output voltage.

Table 1
Comparison between the AMR gradiometer and other gradiometers.

Work	Sensitivity [μV/(nT/m)]	Noise density	Baseline distance (cm)	Integrated
AMR gradiometer	5.7929–11.707	122.36 pT/Hz$^{1/2}$ at 1 Hz	10	Yes
GMI gradiometer[14]	5.94	5 nT/Hz$^{1/2}$ at 5 Hz	6	Yes
Fluxgate gradiometer[16]	—	18 pT/Hz$^{1/2}$ at 1 Hz	60	No
SQUID gradiometer[19]	—	100 fT Hz$^{1/2}$ at 1 Hz	3.5	No
Optically pumped gradiometer[20]	—	10 fT Hz$^{1/2}$ at 1 Hz	2	No

5. Conclusions

In this study, by using an AMR chip sensor along with a signal-conditioning circuit, a vector magnetic gradiometer with adjustable gradient sensitivity was designed for magnetic field gradient measurement, and its structure, measurement principle, and noise performance were analyzed. The instrument was also tested for noise and gradient sensitivity. The experimental results showed that when the feedback resistance is 200 Ω, the noise and nonlinearity of the AMR gradiometer are 122.36 pT/Hz$^{1/2}$ at 1 Hz and 0.9968%, respectively. Under the action of the conditioning circuit, the output voltage of the gradiometer is ±2.5 V. Upon adjusting the feedback resistor R in the *V*/*I* conversion circuit, the adjustable range of the gradient sensitivity of the AMR gradiometer is 5.7929–11.707 μV/(nT/m).

As shown in Table 1, compared with other gradiometers, the output sensitivity of the AMR gradiometer designed in this study has the advantage of being adjustable. From the comparison between the AMR gradiometer and other gradiometers in Table 1, noise performance is found to be not as good as that of the fluxgate and squid gradiometers, and the pT level noise can meet the requirements of nondestructive testing, such as the detection of ferromagnetic metal foreign bodies in solution. In addition, the integrated gradiometer has more advantages in the application field compared with the traditional large-volume gradiometer. In conclusion, the proposed gradiometer can be used to measure the gradient of the input magnetic field, and the imaging of magnetic field anomalies using an 8 × 8 array composed of multiple AMR gradiometers is our future research direction.

References

1 K. Umino, M. Habara, and K. Toko: IEEE J-Stars. **4** (2011) 87. https://doi.org/10.1109/JSTARS.2011.2143696
2 T. Uchiyama and J. Ma: IEEE Trans. Magn. **55** (2019) 1. https://doi.org/10.1109/TMAG.2019.2895399
3 K. Yang, H. Chen, L. Lu, X. Kong, R. Yang, and J. Wang: IEEE Trans. Appl. Supercond. **29** (2019) 1. https://doi.org/10.1109/TASC.2019.2904483
4 E. B. de M. Junior, F. G. Osorio G., F. V. Gutierrez, T. Del Rosso, Tahir, J. G. G. F. Paiva, L. A. F. Mendoza, C. Luz-Lima, E. Yokoyama, A. L. A. Reis, G. Perez, J. de M. Silva, A. C. Bruno, and J. F. D. F. Araujo: Measurement **171** (2021). https://doi.org/10.1016/j.measurement.2020.108808
5 R. E. Bracken and P. J. Brown: 1st Break **23** (2005) 1. https://doi.org/10.3997/1365-2397.23.8.26662
6 R. F. Wiegert: Proc. Spie Int. Society for Optical Engineering (2009). https://doi.org/10.1117/12.818288
7 A. L. Elrefai, I. Sasada, and T. Yoshida: Proc. IEEE Magn. Conf. (INTERMAG) (IEEE, 2015) 1. https://doi.org/10.1109/INTMAG.2015.7156945
8 Q. Li, Z. Shi, Z. Li, H. Fan, G. Zhang, and T. Li: IEEE Sens. J. **21** (2021) 18237. https://doi.org/10.1109/JSEN.2021.3085573
9 X. Wang, H. Liu, H. Wang, J. Ge, H. Dong, and Z. Liu: IEEE Sens. J. **21** (2021) 5952. https://doi.org/10.1109/JSEN.2020.3041001
10 S. Liu, Y. Sui, H. Cheng, Z. Zhang, and D. Clark: IEEE Trans. Instrum. Meas. **70** (2021) 1. https://doi.org/10.1109/TIM.2021.3079559
11 S. Ichihara, N. Mizutani, Y. Ito, and T. Kobayashi: IEEE Trans. Magn. **52** (2016) 1. https://doi.org/10.1109/TMAG.2016.2547364
12 S. Tanaka, T. Akai, Y. Kitamura, Y. Hatsukade, T. Otani, and S. Suzuki: IEEE Trans. Appl. Supercond. **21** (2011) 424. https://doi.org/10.1109/TASC.2010.2080658
13 A. L. Elrefai, I. Sasada, and S. Harada: IEEE Trans. Magn. **51** (2015) 1. https://doi.org/10.1109/TMAG.2015.2453345
14 P. A. D. Riveros, E. C. Silva, S. Pacheco, L. S. B. Cabrera, and C. R. H. Barbosa: IET Sci. Meas. Technol. **14** (2020) 688. https://doi.org/10.1049/iet-smt.2019.0374

15 Y. Sui, H. Miao, Y. Wang, H. Luan, and J. Lin: IEEE Geosci. Remote Sens. **13** (2016) 1837. https://doi.org/10.1109/LGRS.2016.2614538
16 J. M. G. Merayo, P. Brauer, and F. Primdahl: Sens. Actuators, A **120** (2005) 71. https://doi.org/10.1016/j.sna.2004.11.014
17 I. Mateos, J. Ramos-Castro, and A. Lobo: Sens. Actuators, A **235** (2015) 57. https://doi.org/10.1016/j.sna.2015.09.021
18 F. Qiu, J. Wang, Y. Zhang, G. Yang, and C. Weng: Sens. Actuators, A **280** (2018) 61. https://doi.org/10.1016/j.sna.2018.07.031
19 Z. Song, H. Dai, L. Rong, and H. Dong: IEEE Trans. Appl. Supercond. **29** (2019) 1. https://doi.org/10.1109/TASC.2019.2945248
20 O. Alem, R. Mhaskar, R. Jiménez-Martínez, and D. Sheng: Opt. Express **25** (2017) 7849. https://doi.org/10.1364/OE.25.007849

About the Authors

Chao Tan was born in Lichuan, China, in 1982. He received his B.S. and M.S. degrees in measurement control technology and instruments from China University of Geosciences, Wuhan, China, in 2005 and 2008, respectively, and his Ph.D. degree in geological resources and geological engineering from China University of Geosciences in 2011. He is currently an associate professor with the College of Electrical Engineering and New Energy, China Three Gorges University. His interests are in weak magnetic sensors, weak-magnetic-field measurement methods and instrumentation, and weak-signal detection and processes.

Xianzhi Ye was born in Xinyang, Henan, China, in 1998. He is currently pursuing his M.E. degree with the School of Electrical Engineering and New Energy, China Three Gorges University, Yichang, China. He received his B.S. degree in electrical engineering from Wenhua College, Wuhan, China, in 2020. His research interests include weak-magnetic-field measurement methods and magnetic field sensors.

Qihao Sun was born in Liaocheng, Shandong, China, in 1997. He received his B.S. degree in communication engineering from Taishan University, Tai'an, China, in 2020. He is currently pursuing his M.S. degree in control engineering at China Three Gorges University, Yichang, China. His research interests include weak-signal detection and nondestructive testing.

Liang Xin was born in Weifang, Shandong, China, in 1997. He received his B.S. degree in electrical engineering from Shandong Agriculture University, Tai'an, China, in 2020. He is currently pursuing his M.S. degree in control engineering at China Three Gorges University, Yichang, China. His research interests include weak-signal detection and nondestructive testing.

Long Yang was born in Wenzhou, Zhejiang, China, in 1998. He received his B.S. degree in electrical engineering and its automation from Dalian University of Science and Technology, Dalian, China, in 2020. He is currently pursuing his M.S. degree in energy and power engineering at China Three Gorges University, Yichang, China. His research interests include weak-signal detection, crystal frequency drift prediction, and its compensation methods.

Junming Duan was born in Wuhan, Hubei, China, in 1998. He received his B.S. degree in electrical engineering and automation from Huanggang Normal University, Wuhan, in 2020. He is currently pursuing his M.S. degree in energy and power at China Three Gorges University, Yichang, Hubei. His research interests include ground-penetrating radar receivers.

Haoran Chen was born in Yichang, Hubei, China, in 1996. He received his B.S. degree in electrical engineering from China Three Gorges University, Yichang, in 2020, where he is currently pursuing his M.S. degree in energy and power engineering. His research includes the denoising and inversion of unmanned aerial vehicle (UAV) semi-aeronautical transient electromagnetic data received.